

# Enhanced photoelectrochemical performance of CdSe/CdS/TiO<sub>2</sub> nanorod arrays solar cell with a PbS underlayer

Libo Yu · Zhen Li · Yingbo Liu · Fa Cheng ·  
Shuqing Sun

Received: 16 September 2014 / Accepted: 9 January 2015 / Published online: 18 January 2015  
© Springer Science+Business Media New York 2015

**Abstract** Vertically oriented single-crystalline one-dimensional (1D) TiO<sub>2</sub> nanorod arrays film with high aspect ratio was synthesized directly on transparent fluorine-doped tin oxide conducting glass substrate by a facile two-step hydrothermal process. When used in CdSe/CdS/PbS quantum dots sensitized solar cells (QDSSCs), the 1D ordered TiO<sub>2</sub> nanorods with the increased internal surface areas can adsorb more QDs, which enhanced the ability of light absorption. Moreover, 1D ordered TiO<sub>2</sub> nanorods can also offer a direct electrical pathway for photogenerated electrons, accelerating the electrons transfer rate. In addition, the introduction of PbS as underlayer in CdSe/CdS/TiO<sub>2</sub> system can extend the optical absorption range, which greatly raised the utilization of the solar energy. The incident photon to current conversion efficiency of the CdSe/CdS/PbS/TiO<sub>2</sub> nanorods solar cell reached to 52 %, which is higher than that of CdSe/CdS/TiO<sub>2</sub> nanorods solar cell, indicating that the better light harvesting ability could be obtained by the introduction of PbS QDs. The power conversion efficiency of CdSe/CdS/PbS/TiO<sub>2</sub> nanorods solar cell can reach to 2.56 % under one sun illumination (AM 1.5 G, 100 mW/cm<sup>2</sup>), which is greatly higher than that of CdSe/CdS/TiO<sub>2</sub> nanorods solar cell (1.73 %).

## 1 Introduction

Quantum dot sensitized solar cells (QDSSCs) as one of the third generation photovoltaic cells have received much attention in recent years because of their low

manufacturing costs and ease of fabrication [1]. Various narrow band gap semiconductor quantum dots (QDs) such as CdS [2], CdSe [3], PbS [4], and PbSe [5] are commonly used as sensitizers in QDSSCs because of their several attractive advantages, such as the tunable band gap by varying the size of QDs to match the solar spectrum [6], high extinction coefficients that can reduce the dark current [7], large intrinsic dipole moments that lead to rapid charge separation [8], multiple excitons generation (MEG) with a single photon by impact ionization [9], and hot electron injection [10]. Among these semiconductor QDs, CdS and CdSe have been paid much attention due to their appropriate band gap of 2.25 and 1.70 eV in bulk, respectively, which can allow the extension of absorption band to the visible region and show better performance in light harvesting under visible region [11]. Moreover, the co-sensitized structure of CdS and CdSe has been proved to be advantageous over single CdS or CdSe in QDSSCs [12] due to the complementary effect of the two kinds of QDs in light absorption. In addition, lead sulfide (PbS) is a fascinating sensitizer due to its band gap of 0.41 eV [13, 14], which can allow the extension of absorption band to the near infrared (NIR) region of the solar spectrum, leading to the increase the utilization of light. Based on these considerations, it can be anticipated that improved photovoltaic performance of QDSSCs may be achieved with co-sensitization system of CdSe/CdS/PbS QDs.

Nanostructured TiO<sub>2</sub> was usually used as photoanode substrate for QDSSCs because of its several advantages, such as suitable conduction band position, stable chemical and physical properties, and inexpensive cost [15]. In QDSSCs, 1D TiO<sub>2</sub> nanorod arrays can offer direct electronic pathway, accelerating the electrons transport rate and reducing recombination of electrons and holes [16]. However, despite the 1D TiO<sub>2</sub> nanorods possess these

L. Yu · Z. Li · Y. Liu · F. Cheng · S. Sun (✉)  
Department of Chemistry, Tianjin University, Tianjin 300072,  
People's Republic of China  
e-mail: sunshuqing@tju.edu.cn

advantages, one challenge limiting the application of TiO<sub>2</sub> nanorods in QDSSCs is their poor internal surface area for insufficient QDs loading, thus leading to low light harvesting efficiency [17]. In order to address this problem, we have designed 1D TiO<sub>2</sub> nanorods with high aspect ratio, which can provide the increased internal surface areas and improve the QDs loading, leading to the enhancement of power conversion efficiency.

Currently, three methods are commonly used in the QDs deposition on TiO<sub>2</sub>: (1) in situ growth of QDs by chemical bath deposition (CBD) or successive ionic layer adsorption and reaction (SILAR) [18], (2) assemble of presynthesized colloidal QDs with linker molecules [19], (3) deposition of QDs by electrochemical atomic layer epitaxy method (ECALE) [20, 21]. Among these methods, the SILAR is the most widely used method due to the direct contact, high surface coverage of QDs on TiO<sub>2</sub> surface, and easy fabrication process.

In this study, 1D TiO<sub>2</sub> nanorod arrays film with high aspect ratio on FTO glass was successfully fabricated by a facile two-step hydrothermal process and was decorated with multiple QDs (CdSe/CdS/PbS) using SILAR method to form photoanode in QDSSCs. By investigation the J–V performance of the QDSSCs, the solar cell based on CdSe/CdS/PbS/TiO<sub>2</sub> nanorods photoanode exhibited much better photoelectrochemical performance than that of CdSe/CdS/TiO<sub>2</sub> nanorods solar cell.

## 2 Experimental

### 2.1 Synthesis of rutile TiO<sub>2</sub> nanorod arrays on FTO glass

All reagents and chemicals were of analytic grade and used directly in experiments without further purification. In a typical synthesis, Fluorine-doped tin dioxide (FTO) conducting glasses were thoroughly cleaned by ultrasonication in a mixed solution of acetone, 2-propanol, and deionized water (volume ratios of 1:1:1) for 30 min, and finally dried in air.

The 1D single-crystalline TiO<sub>2</sub> nanorod arrays film with high aspect ratio on FTO glass was prepared by a two-step hydrothermal process which is summarized in Fig. 1, details of the fabrication steps are similar to that described

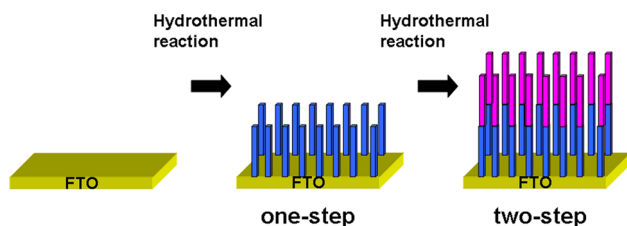


**Fig. 1** Scheme for preparation of 1D TiO<sub>2</sub> nanorod arrays with high aspect ratio

by Liu and Aydil [22]. For the first-step hydrothermal reaction: typically, the well-cleaned FTO conducting glass was transferred to the Teflon-lined stainless steel autoclave at an angle against the wall of the Teflon-liner with the conductive side facing down. Then, a transparent mixed solution consisted of 25 mL of DI water, 30 mL of concentrated hydrochloric acid, 5 mL of saturated NaCl aqueous solution and 1 mL of titanium butoxide was added into the Teflon-lined stainless steel autoclave, filling the 80 % volume of the autoclave. Subsequently, the hydrothermal synthesis reaction was conducted at the temperature of 150 °C for 12 h in an electric oven. After the completion of the first-step hydrothermal reaction, the autoclave was cooled to room temperature under flowing water and the product was taken out, rinsed thoroughly with deionized water and ethanol respectively, and dried in ambient air. For the second-step hydrothermal reaction: the obtained FTO glass from the first-step was placed again in the same Teflon-lined stainless steel autoclave which was filled with freshly prepared growth solution, which is the same as the first-step hydrothermal process. Then the second-step hydrothermal synthesis reaction was conducted at the temperature of 150 °C for another 12 h. After synthesis, the autoclave was cooled to room temperature under flowing water and the product was taken out, rinsed thoroughly with deionized water and ethanol respectively. Finally, the product was dried in ambient air.

### 2.2 Sensitization of CdSe/CdS/PbS QDs onto TiO<sub>2</sub> nanorod arrays electrodes

In situ successive ionic layer adsorption and reaction (SILAR) method [23] was used to form the multiple quantum dots (CdSe/CdS/PbS) onto the TiO<sub>2</sub> nanorod arrays electrode. For sensitization of PbS QDs, the TiO<sub>2</sub> nanorods electrode was dipped in 0.1 M Pb(NO<sub>3</sub>)<sub>2</sub> ethanol solution for 5 min, to allow Pb<sup>2+</sup> ions to adsorb over TiO<sub>2</sub> nanorods structure, and rinsed with ethanol to remove the excess Pb<sup>2+</sup> ions, then dipped for another 5 min into 0.1 M Na<sub>2</sub>S methanol solution to allow S<sup>2-</sup> to react with the Pb<sup>2+</sup>, leading to the formation of PbS, and rinsed again with methanol. The two-step dipping procedure is termed as one SILAR cycle and the incorporated amount of PbS can be increased by repeating the SILAR cycles. For deposition of CdSe/CdS QDs, the PbS-sensitized electrode was initially sensitized with seven cycles of CdS QDs by alternately dipping into 0.1 M Cd(NO<sub>3</sub>)<sub>2</sub> ethanol solution and 0.1 M Na<sub>2</sub>S methanol solution for 5 min. Subsequently, deposition of five cycles of CdSe QDs on CdS/PbS/TiO<sub>2</sub> electrode was conducted by SILAR similar to that of CdS but a longer time (15 min) is required by alternately dipping the sample in Se source and 0.1 M Cd(NO<sub>3</sub>)<sub>2</sub> ethanol solution. Sodium selenosulphate (Na<sub>2</sub>SeSO<sub>3</sub>) aqueous solution which was prepared by refluxing 0.3 M Se in 0.6 M

$\text{Na}_2\text{SO}_3$  at 90 °C for about 6 h is used as the Se source for the deposition of CdSe QDs.

### 2.3 Solar cell fabrication

$\text{Cu}_2\text{S}$  film fabricated on brass foil was selected as the counter electrode, which is prepared by the following procedures: brass foil was immersed into 37 % HCl at 70 °C for 5 min, then rinsed with water and dried in air. After that, the etched brass foil was dipped into 1 M S and 1 M  $\text{Na}_2\text{S}$  aqueous solution, resulting in the formation of a black  $\text{Cu}_2\text{S}$  layer on the foil [6]. The  $\text{Cu}_2\text{S}$  counter electrode and QDs sensitized photoanode were assembled into a sandwich-type configuration using a Scotch spacer ( $\sim 60 \mu\text{m}$  thick) and filled with a droplet of polysulfide electrolyte which consisted of 0.2 M S, 0.6 M  $\text{Na}_2\text{S}$ , and 0.2 M KCl [24] in the co-solvent of water and methanol with volume ratio of 7:3, in which the  $\text{S}^{2-}$  works as holes scavenger [25].

### 2.4 Characterization

The crystal phases of the sample was characterized by X-ray diffraction (XRD), in a  $2\theta$  range from  $10^\circ$  to  $90^\circ$ , using Cu K $\alpha$  radiation ( $\lambda = 1.5416 \text{ \AA}$ ). The morphologies and lattice structures of the samples were examined with field-emission scanning electron microscope (FE-SEM, Nanosem 430 FEL, USA), transmission electron microscopy (TEM, Tecnai G2 F20 FEI, USA), high-resolution TEM (HR-TEM) and selected area electron diffraction (SAED). To prepare TEM samples, the QDs sensitized  $\text{TiO}_2$  nanorods film scraped from the FTO glass was dispersed in ethanol and sonicated, then a few drops of the solution were dropped onto a carbon film supported copper grid. The elemental composition of the sample was analyzed by energy dispersive spectroscopy (EDS). Diffuse reflectance absorption spectra of bare  $\text{TiO}_2$  nanorod arrays and QDs sensitized  $\text{TiO}_2$  nanorod arrays were recorded in the range from 250 to 800 nm by UV–Vis spectrometer. The photocurrent density–voltage ( $J$ – $V$ ) properties of the QDSSCs were obtained under illumination with sunlight simulator at AM 1.5 G ( $100 \text{ mW/cm}^2$ ) condition. The illuminated area of all the QDSSCs was fixed to  $0.16 \text{ cm}^2$  by covering a mask. The incident photon to current conversion efficiency (IPCE) as a function of wavelength was monitored by employing a monochromator to select the illumination wavelength, a 500 W xenon arc lamp (Oriel) served as a light source.

## 3 Results and discussion

### 3.1 Characterization of the $\text{TiO}_2$ nanorod arrays

The crystal phases of the  $\text{TiO}_2$  nanorod arrays electrode have been characterized by X-ray diffraction (XRD), which

is shown in Fig. 2. It can be seen that the as-prepared  $\text{TiO}_2$  nanorod arrays show a tetragonal rutile structure (JCPDS no. 21-1276) after the hydrothermal reaction. Compared with the intensity of (101) and (112) diffraction peaks in XRD patterns of the as-prepared  $\text{TiO}_2$ , the enhanced (002) peak indicates that the nanorods are well crystallized and grow in (001) direction with the growth axis parallel to the substrate surface.

The 1D  $\text{TiO}_2$  nanorod arrays with high aspect ratio on FTO glass were synthesized using a two-step hydrothermal process. Figure 3a presents the top morphology of the product obtained from the first-step hydrothermal reaction. The top facets of  $\text{TiO}_2$  nanorods are square, which shows the typical growth habit of the tetragonal crystal structure. Moreover, many step edges are present at the top surfaces of the  $\text{TiO}_2$  nanorods, which can serve as nucleation sites for the further growth of nanorods when conducting the second-step hydrothermal process. Figure 3b shows the cross-sectional view of the corresponding sample, showing that the  $\text{TiO}_2$  nanorods are highly ordered and nearly perpendicular to the FTO glass with the length of around  $3 \mu\text{m}$ . Figure 3c shows the top FE-SEM image of the  $\text{TiO}_2$  nanorod arrays obtained from the two-step hydrothermal process. Obviously, the morphology of the top surface for the  $\text{TiO}_2$  nanorods has not changed very much comparing with that of the  $\text{TiO}_2$  nanorods obtained from the one-step hydrothermal reaction in Fig. 3a. In order to investigate the influence of two-step hydrothermal process on the width variation of nanorods, the image analysis software ImageJ has been employed to estimate the average width of the nanorods obtained from the one-step and two-step hydrothermal process, respectively. The analysis results showed that the average width of nanorods obtained from these two different hydrothermal processes is around 197 and 199 nm respectively, indicating that the second hydrothermal

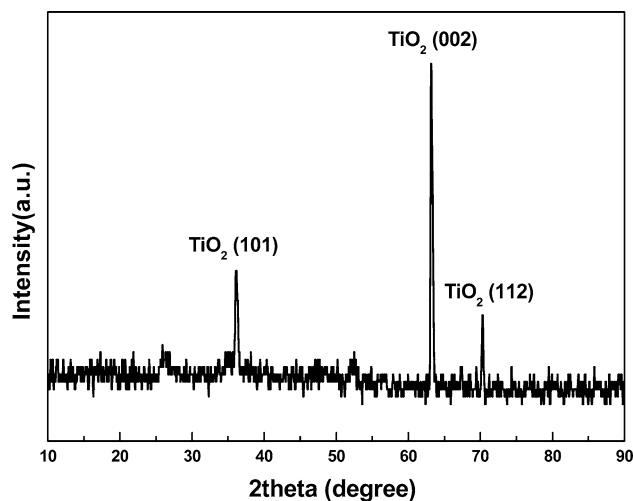
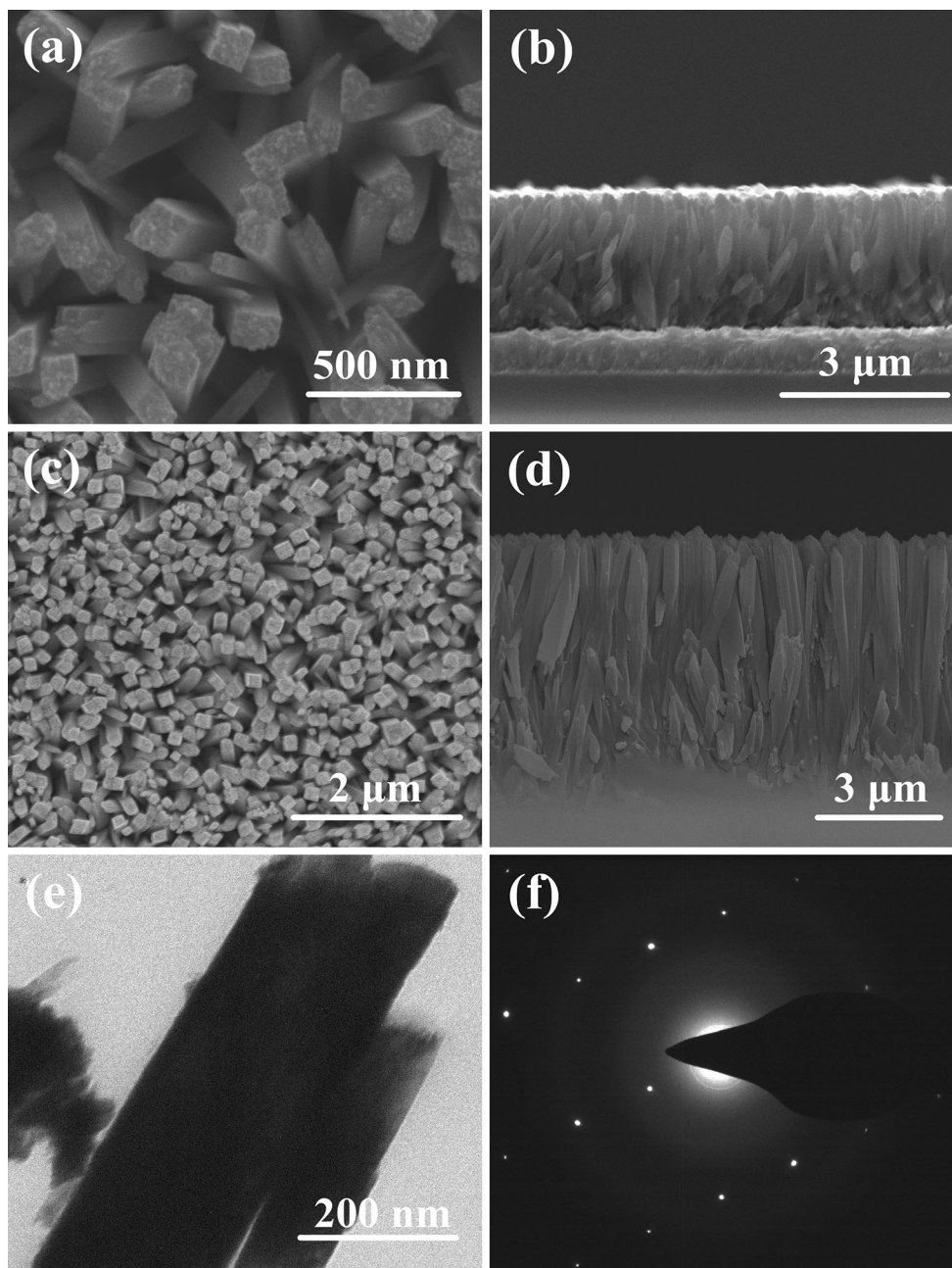


Fig. 2 XRD pattern of  $\text{TiO}_2$  nanorod arrays

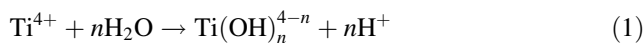


**Fig. 3** FE-SEM images of TiO<sub>2</sub> nanorod arrays film: **a** top view and **b** cross-sectional view of the first hydrothermal reaction; **c** top view and **d** cross-sectional view of the second hydrothermal reaction.

process has little influence on the average width variation of the nanorods. However, the cross-sectional FE-SEM image of the TiO<sub>2</sub> nanorod arrays shown in Fig. 3d after the two-step hydrothermal process displays that the length of nanorod is nearly doubled to around 6 μm comparing with that of nanorods obtained from the first hydrothermal reaction in Fig. 3b, indicating that the second step hydrothermal process can enlarge the length of nanorods without changing their width. The main chemical reaction responsible for the formation of the TiO<sub>2</sub> nanorod arrays during

**e** TEM image of a single TiO<sub>2</sub> nanorod and **f** SAED pattern of the corresponding structure

this two-step hydrothermal process can be described as follows [26].



The Ti(IV) oxo species is assumed to be an intermediate between TiO<sup>2+</sup> and TiO<sub>2</sub>, consisting of partly dehydrated polymeric Ti(IV) hydroxide [27]. The acid condition could slow down the hydrolysis reaction of Ti(OC<sub>4</sub>H<sub>9</sub>)<sub>4</sub> by



providing free  $H^+$  as present in reaction (1), which is necessary for the growth of oriented 1D  $TiO_2$  nanorods. Meanwhile,  $Cl^-$  provided by saturated NaCl could preferentially adsorb on rutile (110) plane and retard the growth rate of (110) surface, resulting in the suppression of lateral growth, which will facilitate the anisotropic growth of rutile nanorods along (001) orientation [28]. Therefore, the  $TiO_2$  nanorod arrays can grow taller without changing the top surface morphology during the second hydrothermal reaction, resulting in an increase in the surface area, which is beneficial for the more adsorption of QDs. The TEM image of a single  $TiO_2$  nanorod and the corresponding SAED pattern are shown in Fig. 3e, f. The well-aligned spots exhibited in the SAED pattern indicate that the  $TiO_2$  nanorod is single crystalline.

### 3.2 Characterization of CdSe/CdS/PbS/ $TiO_2$ nanorod arrays

After sensitization with multiple quantum dots (CdSe/CdS/PbS), the ordered  $TiO_2$  nanorod arrays structure is retained, as shown in Fig. 4a. It is obvious that the surface of  $TiO_2$  nanorod became rougher than that of bare  $TiO_2$  nanorod (Fig. 3a), which means that the QDs had covered on the surface of  $TiO_2$  nanorod after SILAR. The composition of the QDs sensitized  $TiO_2$  nanorods electrode and the corresponding quantitative data were analyzed by energy dispersive spectroscopy (EDS) equipped on transmission electron microscope (TEM), which is shown in Fig. 4b. Apart from C and Cu elements that came from carbon film supported on the copper grid, the appearance of Ti and O peaks indicates that the supporter material of the electrode is  $TiO_2$ . Other elements peaks including Se, Pb, S, and Cd can also be observed in the EDS spectrum of the QDs sensitized  $TiO_2$  nanorods, confirming that PbS, CdS and CdSe are successfully assembled onto the  $TiO_2$  nanorods.

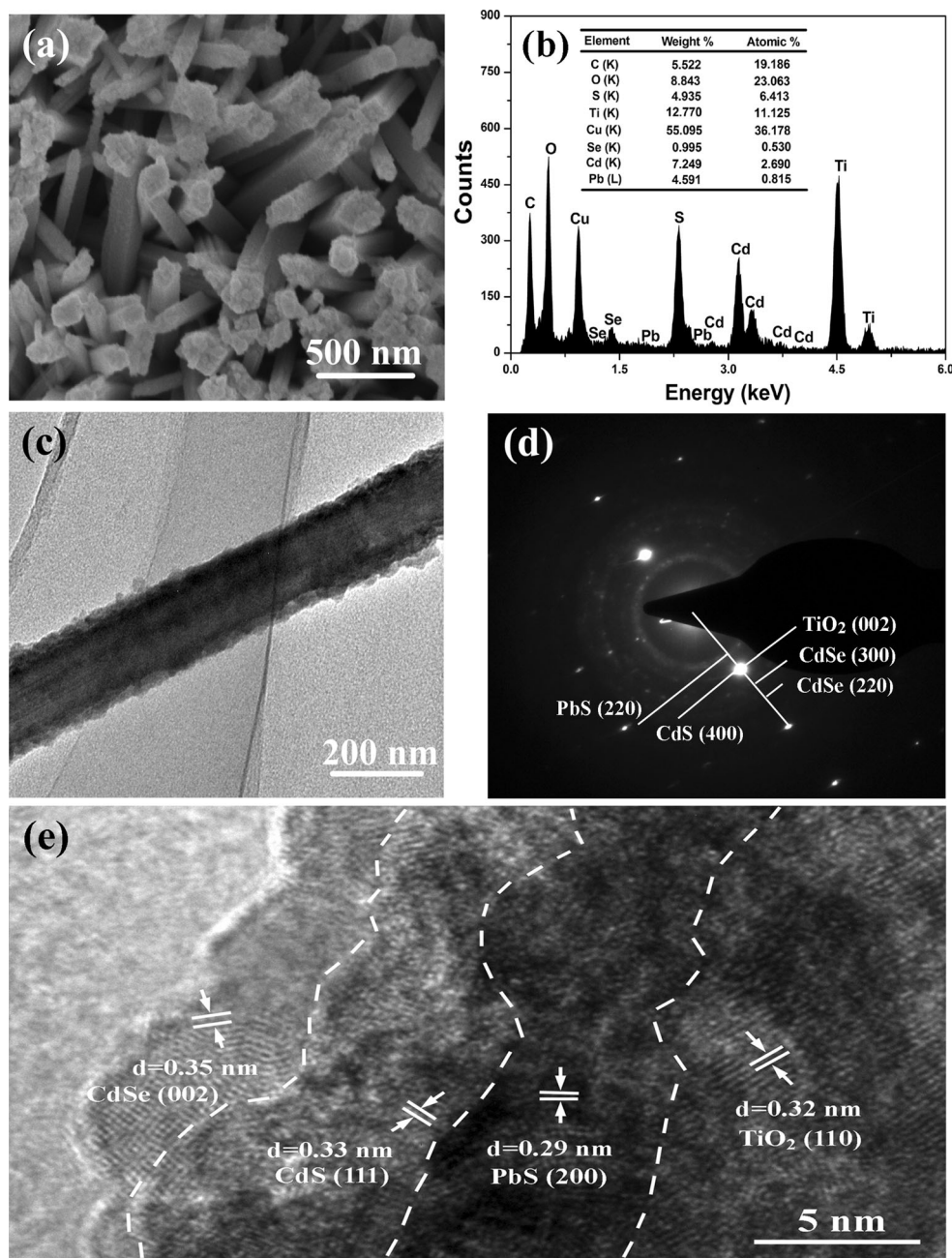
The detailed microscopic characterization of the CdSe/CdS/PbS/ $TiO_2$  nanorods has been performed by TEM, high-resolution TEM (HR-TEM), and selected area electron diffraction (SAED). The typical TEM image of a  $TiO_2$  nanorod deposited with CdSe/CdS/PbS is shown in Fig. 4c, it can be seen clearly that the surface of  $TiO_2$  nanorod is covered with a number of nanoparticles. Figure 4d shows the SAED pattern of the corresponding structure in Fig. 4c, apart from the well-aligned spots which come from the single-crystalline  $TiO_2$  nanorod, the diffraction rings originate from polycrystalline of CdSe/CdS/PbS QDs can be identified in this SAED pattern, implying the successful deposition of QDs on the  $TiO_2$  nanorods. Figure 4e shows the HR-TEM image of the CdSe/CdS/PbS/ $TiO_2$  nanorod. The clear lattice fringes indicated high crystallinity of  $TiO_2$ , PbS, CdS and CdSe. A lattice spacing measured for the crystalline plane is 0.32 nm, which can be assigned to

the interplanar distance of rutile  $TiO_2$  (110) (JCPDS no. 21-1276). Among the crystal planes of rutile  $TiO_2$ , the (110) plane possesses the lowest surface energy [29]. According to the crystal growth theory, the planes with lower surface energies generally grow slowly and tend to survive during the growth [30]. Therefore, the (110) plane of the rutile  $TiO_2$  can be obviously observed in the HR-TEM photographs. Around the rutile  $TiO_2$  crystalline edge, other fine crystallines can be distinguished. By carefully measuring the lattice parameters and comparing with the data in JCPD, the crystallites with lattice spacing of 0.29 nm connecting to  $TiO_2$ , can be ascribed to the (200) plane of PbS (JCPDS no. 05-0592). The lattice fringes with interplanar spacing of 0.33 nm connecting to PbS can be ascribed to the (111) plane of CdS (JCPDS no. 10-0454), and the outer crystalline adjacent to the CdS layer with lattice spacing of 0.35 nm corresponds to the (002) plane of CdSe (JCPDS no. 08-0459). These results provide powerful evidence that the QDs covered on  $TiO_2$  nanorods are composed of PbS, CdS and CdSe QDs.

### 3.3 Optical properties of QDs sensitized $TiO_2$ nanorod arrays

The UV–Vis Diffuse reflectance absorption spectra were used to record the difference light absorption properties of bare  $TiO_2$  nanorods (two-step), CdS/ $TiO_2$  nanorods (two-step), CdSe/ $TiO_2$  nanorods (two-step), CdSe/CdS/ $TiO_2$  nanorods (two-step), CdSe/CdS/PbS/ $TiO_2$  nanorods (one-step) and CdSe/CdS/PbS/ $TiO_2$  nanorods (two-step) electrodes. As shown in Fig. 5, the absorption edge of bare  $TiO_2$  nanorods (two-step) electrode (spectrum a, Fig. 5) occurs at around 405 nm and the main light absorption centered on ultraviolet light region, this can be ascribed to the wide band gap of rutile  $TiO_2$  (3.0 eV) [31]. Compared with the absorption spectra of the bare  $TiO_2$  nanorods (two-step) electrode, the absorption edges of the CdS/ $TiO_2$  nanorods (two-step) and CdSe/ $TiO_2$  nanorods (two-step) electrodes were enlarged to 530 nm (spectrum b, Fig. 5) and 600 nm (spectrum c, Fig. 5), corresponding to the calculated band gaps of 2.34 and 2.07 eV for CdS and CdSe, respectively. The calculated band gaps are higher than the values of bulk CdS (2.25 eV) and CdSe (1.70 eV), indicating that the sizes of CdS and CdSe deposited on the  $TiO_2$  nanorods (two-step) film are within the scale of QDs. According to the empirical equations given by Yu et al. [32], the average diameters of CdS and CdSe QDs were estimated to be 9.4 and 4.6 nm, respectively. For the CdSe/CdS/ $TiO_2$  nanorods (two-step) electrode (spectrum d, Fig. 5), a red-shift in the absorption with onset around 650 nm can be observed compared to the absorption spectrum of CdSe/ $TiO_2$  nanorods (two-step) electrode. It is worth noting that the absorption range of CdSe/CdS/PbS/

**Fig. 4** **a** FE-SEM image of CdSe/CdS/PbS/TiO<sub>2</sub> nanorods electrode and **b** EDS spectra of corresponding electrode. **c** TEM image of CdSe/CdS/PbS/TiO<sub>2</sub> nanorod electrode and **d** SAED pattern of the corresponding structure; **e** HR-TEM image of CdSe/CdS/PbS/TiO<sub>2</sub> nanorod electrode



TiO<sub>2</sub> nanorods (two-step) electrode (spectrum f, Fig. 5) is further extended to around 700 nm compared to that of CdSe/CdS/TiO<sub>2</sub> nanorods electrode, which indicate that introduction of PbS in CdSe/CdS/TiO<sub>2</sub> system can extend the optical absorption range, thus improving the ability of light harvesting. In addition, compared with the absorption spectrum of CdSe/CdS/PbS/TiO<sub>2</sub> nanorods (one-step) electrode (spectrum e, Fig. 5), the CdSe/CdS/PbS/TiO<sub>2</sub> nanorods (two-step) electrode (spectrum f, Fig. 5) also shows a red shift in the absorption and an increased absorbance, which can be ascribed to that TiO<sub>2</sub> nanorods obtained from two-step hydrothermal reaction provided a

larger surface areas and could adsorb more QDs than the TiO<sub>2</sub> nanorods obtained from one-step hydrothermal reaction.

### 3.4 Photoelectrochemical characterization

The photocurrent density–voltage (J–V) curves of QDSSCs assembled with different photoanodes were measured by Oriol I–V test station under one sun condition (AM 1.5 G, 100 mW/cm<sup>2</sup>) with the active area of 0.16 cm<sup>2</sup>. The influence of the SILAR cycles of PbS as underlayer beneath CdSe/CdS on the J–V characteristics of CdSe/CdS/

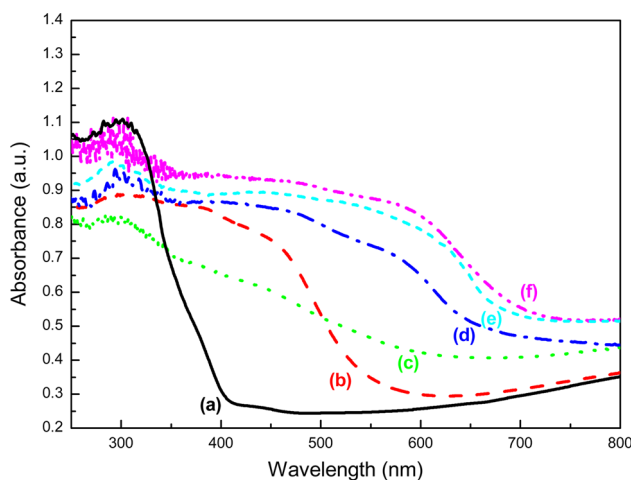


**Fig. 5** Diffuse reflectance absorption spectra of *a* bare TiO<sub>2</sub> nanorods (two-step) film, *b* CdS/TiO<sub>2</sub> nanorods (two-step) film, *c* CdSe/TiO<sub>2</sub> nanorods (two-step) film, *d* CdSe/CdS/TiO<sub>2</sub> nanorods (two-step) film, *e* CdSe/CdS/PbS/TiO<sub>2</sub> nanorods (one-step) film, and *f* CdSe/CdS/PbS/TiO<sub>2</sub> nanorods (two-step) film

PbS/TiO<sub>2</sub> nanorods solar cells are displayed in Fig. 6. It is found that both the short-circuit current density ( $J_{sc}$ ) and open-circuit voltage ( $V_{oc}$ ) increased gradually with the increase of the PbS QDs cycles at initial stage (from 1 cycle to 2 cycles), and the optimum values of these two parameters (14.18 mA/cm<sup>2</sup>, 0.43 V) could be obtained by 2 SILAR cycles of PbS. Then further increase of SILAR cycles of PbS QDs (3 cycles) lead to the reduction of the  $J_{sc}$  and  $V_{oc}$ . The power conversion efficiency ( $\eta$ ) as a function of SILAR cycles of PbS is summarized in the inset of Fig. 6, it can be observed that 2 cycles of PbS make the CdSe/CdS/PbS/TiO<sub>2</sub> nanorods solar cell exhibit the maximum  $\eta$  of 2.56 %.

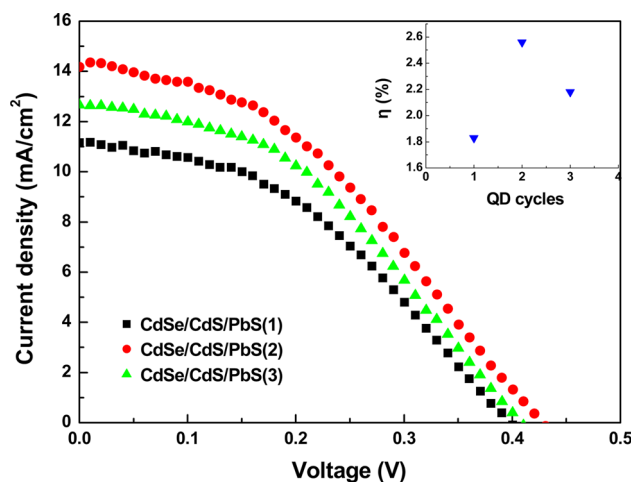


**Fig. 6** J–V characteristics of CdSe/CdS/PbS solar cells based on TiO<sub>2</sub> nanorods obtained from two-step hydrothermal process. The inset shows the power conversion efficiency as a function of the cycles of PbS underlayer

In order to demonstrate that introduction of PbS in CdSe/CdS/TiO<sub>2</sub> system and 1D TiO<sub>2</sub> nanorods with high aspect ratio (the length increased while the width remained the same) structure obtained from two-step hydrothermal process have important effect for improving the performance of QDSSCs, we also prepared CdSe/CdS QDSSC based on TiO<sub>2</sub> nanorods which obtained from two-step hydrothermal process and CdSe/CdS/PbS(2) QDSSC based on TiO<sub>2</sub> nanorods which obtained from one-step hydrothermal process as control experiments. Figure 7 depicts the J–V behaviors of QDSSCs based on CdSe/CdS/PbS(2)/TiO<sub>2</sub> nanorods (two-step), CdSe/CdS/TiO<sub>2</sub> nanorods (two-step), and CdSe/CdS/PbS(2)/TiO<sub>2</sub> nanorods (one-step) electrodes, respectively. The corresponding photovoltaic performance parameters of these solar cells including short-circuit current density ( $J_{sc}$ ), open-circuit voltage ( $V_{oc}$ ), fill factor (FF), and power conversion efficiency ( $\eta$ ) are listed in Table 1. In contrast with CdSe/CdS/TiO<sub>2</sub> nanorods (two-step) solar cell, both the  $J_{sc}$  and  $V_{oc}$  of CdSe/CdS/PbS(2)/TiO<sub>2</sub> nanorods (two-step) solar cell are increased, resulting in the enhancement of power conversion efficiency from 1.73 to 2.56 %, showing that introduction of PbS underlayer in CdSe/CdS/TiO<sub>2</sub> system is favorable for the improvement of the solar cell performance. This can be attributed to the extension of optical absorption range and the enhancement of light harvesting efficiency provided by PbS QDs. In addition, compared with CdSe/CdS/PbS(2)/TiO<sub>2</sub> nanorods (one-step) solar cell, all the photovoltaic performance parameters in CdSe/CdS/PbS(2)/TiO<sub>2</sub> nanorods (two-step) solar cell are increased, showing that the TiO<sub>2</sub> nanorods with longer length obtained from two-step hydrothermal process is advantageous to boost the power conversion

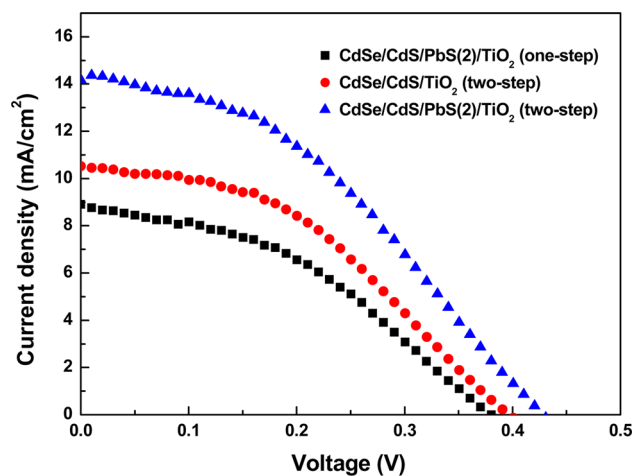


**Fig. 7** J–V curves of QDSSCs assembled with CdSe/CdS/PbS(2)/TiO<sub>2</sub> nanorods (one-step hydrothermal), CdSe/CdS/PbS(2)/TiO<sub>2</sub> nanorods (two-step hydrothermal), and CdSe/CdS/TiO<sub>2</sub> nanorods (two-step hydrothermal) electrodes measured under AM 1.5 G condition

**Table 1** Photovoltaic parameters of QDSSCs assembled with different photoanodes

Samples	$J_{sc}$ (mA/cm <sup>2</sup> )	$V_{oc}$ (V)	FF	$\eta$ (%)
CdSe/CdS/PbS(2)/TiO <sub>2</sub> (two-step)	14.18	0.43	0.42	2.56
CdSe/CdS/TiO <sub>2</sub> (two-step)	10.53	0.40	0.41	1.73
CdSe/CdS/PbS(2)/TiO <sub>2</sub> (one-step)	8.91	0.38	0.40	1.35

efficiency. The contribution of the TiO<sub>2</sub> nanorods obtained from two-step hydrothermal reaction to the enhanced power conversion efficiency may be ascribed to two aspects. For one thing, the length of TiO<sub>2</sub> nanorods is increased while the width remains unchanged through two-step hydrothermal process, which lead to a higher aspect ratio than the TiO<sub>2</sub> nanorods obtained from one-step growth, resulting in an increased internal surface areas to adsorb more QDs to enhance the light-harvesting efficiency; for another, highly ordered TiO<sub>2</sub> nanorods offer the direct transport pathways for photogenerated electrons, which can accelerate the electrons transfer rate and reduce the recombination of electrons and holes.

The incident photon to current conversion efficiency (IPCE) spectra of QDSSCs based on CdSe/CdS/TiO<sub>2</sub> nanorods (two-step) and CdSe/CdS/PbS(2)/TiO<sub>2</sub> nanorods (two-step) photoanodes are presented in Fig. 8. The light response revealed by the IPCE spectra of CdSe/CdS/TiO<sub>2</sub> nanorods and CdSe/CdS/PbS/TiO<sub>2</sub> nanorods solar cells exhibit similar trends to their corresponding UV–Vis spectra in Fig. 5. The maximum IPCE values obtained from CdSe/CdS/PbS(2)/TiO<sub>2</sub> nanorods solar cell is around 52 %, which is higher than that of CdSe/CdS/TiO<sub>2</sub> nanorods solar cell (40 %). The improvement of the IPCE can be ascribed to the introduction of PbS underlayer, which can extend the light response region compared to that of

CdSe/CdS/TiO<sub>2</sub> nanorods solar cell, resulting in more light was involved in generation of photocurrent.

Figure 9 shows the photoelectrical conversion structure of our CdSe/CdS/PbS/TiO<sub>2</sub> nanorods solar cell, which consists of TiO<sub>2</sub> nanorods obtained from two-step hydrothermal process, CdSe/CdS/PbS QDs sensitizer, polysulfide electrolyte, and Cu<sub>2</sub>S counter electrode. Under illumination, photons are captured by QDs, yielding electro-hole pairs. The electrons are rapidly injected into the TiO<sub>2</sub> nanorod arrays film, simultaneously, the remaining holes are scavenged to the counter electrode via a hole transporting redox couple comprising of polysulfide electrolyte. From illustration of the working mechanism of QDSSC in Fig. 9, it can be found that the utilization of light, amount of QDs adsorbed on TiO<sub>2</sub> nanorods, and electron transport are the key factors affecting the performance of QDSSC. Introduction of PbS in CdSe/CdS/TiO<sub>2</sub> system can broaden the optical absorption area, making more light get involved in the process of photon-to-electron conversion. The TiO<sub>2</sub> nanorods with increased length acquired by two-step hydrothermal process possess high aspect ratio and high internal surface areas, which are advantageous for adsorbing of more QDs on its surface, leading to the improvement of light harvesting efficiency. In addition, the highly ordered single-crystalline 1D TiO<sub>2</sub> nanorod arrays can offer a direct electrical pathway for photogenerated electrons, which can increase the electron transport rate and effectively suppress the recombination of electrons and holes. Thus, it could be concluded that our CdSe/CdS/PbS/TiO<sub>2</sub> nanorods solar cell is of great potential for designing high efficiency solar cells.

The stability of CdSe/CdS/PbS(2)/TiO<sub>2</sub> nanorods solar cell has been monitored at different time intervals, and the results are shown in Fig. 10. It is found that about 0.8 % degradation of  $\eta$  is observed after 120 min, which demonstrated an excellent stability of the solar cell during the measurement. Although an acceptable power conversion efficiency of 2.56 % has achieved with QDSSC based on CdSe/CdS/PbS(2)/TiO<sub>2</sub> nanorods electrode, it is reasonable to anticipate that there is much room for further improvement of the power conversion efficiency, especially by developing appropriate counter electrode materials or finding more suitable redox electrolyte for holes scavenging to reduce recombination. These challenges will be the focus of our continuous research work.

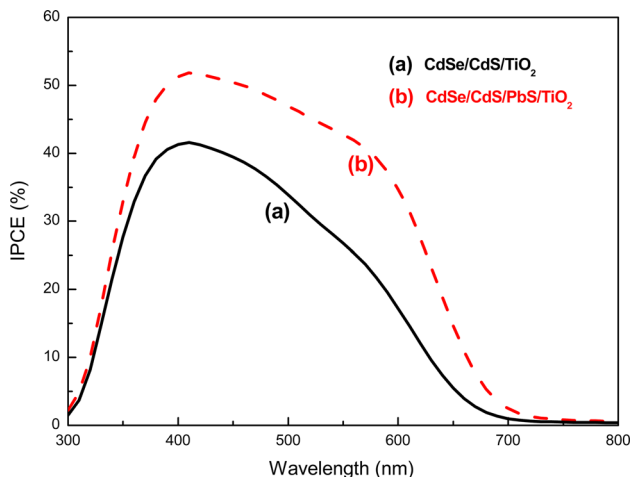


**Fig. 8** IPCE spectra of QDSSCs assembled with CdSe/CdS/TiO<sub>2</sub> nanorods and CdSe/CdS/PbS(2)/TiO<sub>2</sub> nanorods photoanodes



**Fig. 9** Schematic diagram of the photoelectrical conversion configuration of CdSe/CdS/PbS/TiO<sub>2</sub> nanorods solar cell

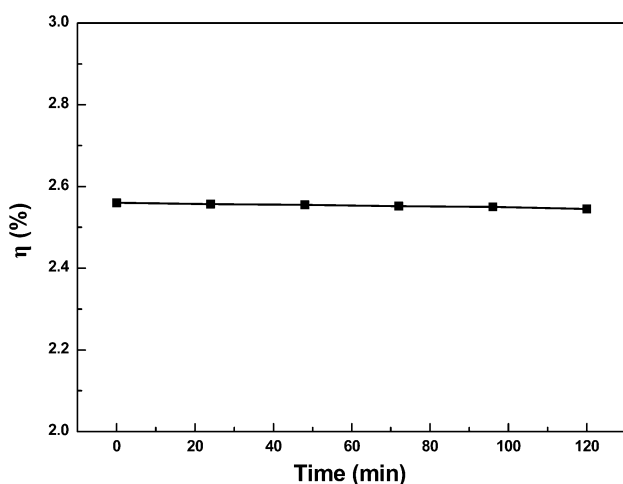
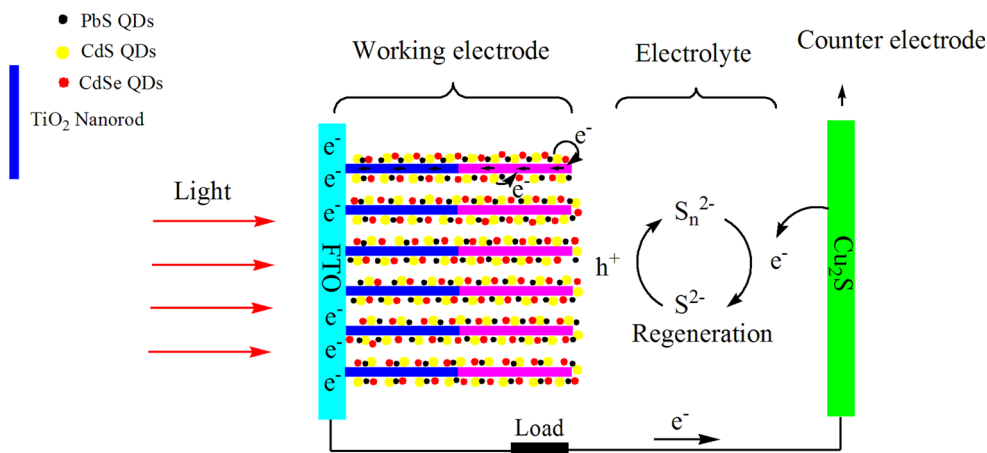


**Fig. 10** Variation of the power conversion efficiency of CdSe/CdS/PbS(2)/TiO<sub>2</sub> nanorods solar cell as a function of time

#### 4 Conclusions

In summary, the single-crystalline 1D TiO<sub>2</sub> nanorod arrays with high aspect ratio directly grown on FTO glass have been successfully synthesized using a facile two-step hydrothermal process. The CdSe/CdS/PbS QDs have been assembled onto TiO<sub>2</sub> nanorods film by SILAR and used as photoanode in solar cell. The short-circuit current density of 14.18 mA/cm<sup>2</sup>, the open-circuit voltage of 0.43 V, and the power conversion efficiency of 2.56 % were achieved with CdSe/CdS/PbS/TiO<sub>2</sub> nanorods (two-step) solar cell, which was significantly higher than that of CdSe/CdS/TiO<sub>2</sub> nanorods (two-step) solar cell and CdSe/CdS/PbS/TiO<sub>2</sub> nanorods (one-step) solar cell, showing that the introduction of PbS underlayer in CdSe/CdS/TiO<sub>2</sub> system and 1D TiO<sub>2</sub> nanorod arrays with increased length can improve the performance of QDSSCs. The acceptable power conversion efficiency of our CdSe/CdS/PbS/TiO<sub>2</sub> nanorods solar cell has demonstrated that its significance in designing high efficiency QDSSCs.

**Acknowledgments** The authors gratefully acknowledge the support for this work from the Key project of Tianjin Sci-Tech Support Program (No. 08ZCKFH01400).

#### References

1. Y.-L. Lee, Y.-S. Lo, *Adv. Funct. Mater.* **19**, 604 (2009)
2. X. Gu, D. Song, Y. Zhao, Y. Qiang, *J. Mater. Sci. Mater. Electron.* **24**, 3009 (2013)
3. B. Mukherjee, Y.R. Smith, V. Subramanian, *J. Phys. Chem. C* **116**, 15175 (2012)
4. Y. Tu, J. Wu, Z. Lan, Y. Lin, Q. Liu, B. Lin, G. Liu, *J. Mater. Sci. Mater. Electron.* **25**, 3016 (2014)
5. N. Guijarro, T. Lana-Villarreal, T. Lutz, S.A. Haque, R. Gómez, *J. Phys. Chem. Lett.* **3**, 3367 (2012)
6. J. Tian, R. Gao, Q. Zhang, S. Zhang, Y. Li, J. Lan, X. Qu, G. Cao, *J. Phys. Chem. C* **116**, 18655 (2012)
7. S. Emin, S.P. Singh, L. Han, N. Satoh, A. Islam, *Sol. Energy* **85**, 1264 (2011)
8. E.M. Barea, M. Shalom, S. Giménez, I. Hod, I. Mora-Seró, A. Zaban, J. Bisquert, *J. Am. Chem. Soc.* **132**, 6834 (2010)
9. M.C. Beard, *J. Phys. Chem. Lett.* **2**, 1282 (2011)
10. W.A. Tisdale, K.J. Williams, B.A. Timp, D.J. Norris, E.S. Aydil, X.Y. Zhu, *Science* **328**, 1543 (2010)
11. G. Zhu, L. Pan, T. Xu, Z. Sun, *ACS Appl. Mater. Interfaces* **3**, 3146 (2011)
12. M. Li, Y. Liu, H. Wang, H. Shen, W. Zhao, H. Huang, C. Liang, *J. Appl. Phys.* **108**, 094304 (2010)
13. J. Kim, H. Choi, C. Nahm, C. Kim, J.I. Kim, W. Lee, S. Kang, B. Lee, T. Hwang, H.H. Park, B. Park, *Appl. Phys. Lett.* **102**, 183901 (2013)
14. S.D. Sung, I. Lim, P. Kang, C. Lee, W.I. Lee, *Chem. Commun.* **49**, 6054 (2013)
15. D.H. Kim, W.M. Seong, I.J. Park, E.S. Yoo, S.S. Shin, J.S. Kim, H.S. Jung, S. Lee, K.S. Hong, *Nanoscale* **5**, 11725 (2013)
16. Ö. Kerkez, İ. Boz, *React. Kinet. Mech. Catal.* **110**, 543 (2013)
17. H. Yu, J. Pan, Y. Bai, X. Zong, X. Li, L. Wang, *Chem. Eur. J.* **19**, 13569 (2013)
18. C. Wang, Z. Jiang, L. Wei, Y. Chen, J. Jiao, M. Eastman, H. Liu, *Nano Energy* **1**, 440 (2012)
19. H. Wang, C. Luan, X. Xu, S.V. Kershaw, A.L. Rogach, *J. Phys. Chem. C* **116**, 484 (2012)
20. J. Zhang, J. Yang, M. Liu, G. Li, W. Li, S. Gao, Y. Luo, *J. Electrochem. Soc.* **161**, D55 (2013)

21. S. Feng, J. Yang, M. Liu, H. Zhu, J. Zhang, G. Li, J. Peng, Q. Liu, *Electrochim. Acta* **83**, 321 (2012)
22. B. Liu, E.S. Aydil, *J. Am. Chem. Soc.* **131**, 3985 (2009)
23. H. Lee, M. Wang, P. Chen, D.R. Gamelin, S.M. Zakeeruddin, M. Grätzel, M.K. Nazeeruddin, *Nano Lett.* **9**, 4221 (2009)
24. Y. Lai, Z. Lin, D. Zheng, L. Chi, R. Du, C. Lin, *Electrochim. Acta* **79**, 175 (2012)
25. V. Chakrapani, D. Baker, P.V. Kamat, *J. Am. Chem. Soc.* **133**, 9607 (2011)
26. J. Zhou, G. Zhao, G. Han, B. Song, *Ceram. Int.* **39**, 8347 (2013)
27. E. Hosono, S. Fujihara, K. Kakiuchi, H. Imai, *J. Am. Chem. Soc.* **126**, 7790 (2004)
28. K. Kakiuchi, E. Hosono, H. Imai, T. Kimura, S. Fujihara, *J. Cryst. Growth* **293**, 541 (2006)
29. U. Diebold, *Appl. Phys. A Mater. Sci. Process.* **76**, 681 (2003)
30. M. Gao, Y. Li, M. Guo, M. Zhang, X. Wang, *J. Mater. Sci. Technol.* **28**, 577 (2012)
31. M. Xu, P. Da, H. Wu, D. Zhao, G. Zheng, *Nano Lett.* **12**, 1503 (2012)
32. W.W. Yu, L. Qu, W. Guo, X. Peng, *Chem. Mater.* **15**, 2854 (2003)